

Variation of the second-phase morphology and its influence on fracture behavior of Al-Si alloy

Sun Yu^{1,2} Chen Jin¹ Sun Guoxiong¹

(¹ Department of Materials Science and Engineering, Southeast University, Nanjing 210096, China)

(² Department of Materials Science and Engineering, Yancheng Institute of Technology, Yancheng 224002, China)

Abstract: Using an optical microscope and scanning electron microscope (SEM), the variation of eutectic Si morphology of Al-Si alloy in solution treatment was observed to study its influence on mechanical properties and fracture behavior. The results show that eutectic Si undergoes stubbing, necking, fragmentation, and growth in the initial stage (250 min); in the middle solution stage (250 to 400 min), the eutectic Si morphology has no significant change, only the degree of spheroidizing becomes higher; after 600 min, the growth of eutectic Si is a coarsening process controlled by diffusion and follows the Lifshitz-Slyozov-Wagner (LSW) model, and the eutectic Si morphology deteriorates due to the occurrence of facets and lap. Based on the quantitative measure and regression analysis, the eutectic Si morphology has a remarkable influence on mechanical properties and fracture behavior.

Key words: Al-Si alloy; variation of Si phase; mechanical properties; fracture behavior

Al-Si alloys are the most important Al-based casting alloys because of their excellent castability, low shrinkage, high corrosion resistance, good weldability, and low thermal expansion, and are widely used in the electrical, automobile and aircraft industries^[1-3]. As the second-phase in Al-Si alloy, Si has a close relation with the mechanical properties of alloys. Research indicates that the finer, rounded and evenly distributed Si particles tend to improve the stress field atmosphere between elastic rigid particles (Si particle) and ductile Al-matrix, which remarkably increases the mechanical properties^[4-10]. Much attention has been paid to controlling the eutectic Si morphology in recent years. The eutectic Si in unmodified Al-Si alloy is presented as coarse flakes, which have a detrimental effect on the ductility. However, the minor additions of Na or Sr to alloys can cause morphological transition of eutectic Si from coarse flakes to fine fibers, which have a pronounced increase in the mechanical properties of Al-Si alloy, especially to the fracture elongation^[11-14]. Similarly, the influence of solution heat treatment on mechanical properties of Al-Si-Mg (Cu) alloys has been widely investigated^[15-19]. During solution treatment alloying elements dissolve to produce a homogeneous solid solution and the morphology of eutectic Si undergoes progressive changes; aging causes the precipitation of the strengthening phase (such as Mg₂Si or CuAl₂)

within the primary α (Al) dendrite. Previous research mainly focuses on the precipitation sequence and variation of the strengthening phase during solution heat treatment. The effect of sole eutectic Si morphology on mechanical properties and fracture behavior has rarely been studied.

There are two different views about the variation of the eutectic Si morphology in the solution treatment. One holds that in sand cast modified A356 alloys, a major fraction of Si has spheroidized after only 50 min of solution time, and a fully spheroidized structure is observed in modified permanent mold after only 25 min of solution time^[17]. However, the other argues that, with the help of the scanning electron microscope (SEM), the Si particles were interconnected, 3-D, and pointed out that the fragmentation and spheroidization of eutectic Si, which was inferred based upon the 2-D observation, actually did not occur^[19].

The present work is to further investigate the variation of eutectic Si morphology in the solution treatment and the relationship between the morphology of eutectic Si with the mechanical properties and fracture behavior of Al-Si alloy.

1 Experimental Procedure

1.1 Preparation of experimental alloy and solution treatment

The experimental alloy with a nominal composition Al-12.35% Si alloy (ZAlSiD-0) was melted in an electrical resistance furnace using graphite crucible.

Received 2003-10-21.

Biographies: Sun Yu (1963—), male, graduate, associate professor; Sun Guoxiong (corresponding author), male, professor, gxsun@seu.edu.cn.

Al-10%Sr master alloy was introduced to the melt at 750 °C with slight stirring. After holding for 30 min, SW-RJ-1 flux was added for degassing. Then, the melt was poured at 720°C into a standard tensile sample mold (grey iron, preheated at 250 °C). The as-cast samples (12 mm in diameter, 60 mm in gage length) were solution treated in a resistance-heated muffle furnace for 20 to 2 000 min at $(535 \pm 5)^\circ\text{C}$, then quenched in water at room temperature.

1.2 Mechanical property test and metallographic observation

Tensile properties were evaluated using a universal tensile testing machine (WJ-10) at a constant rate of 0.1 mm/s. Five tensile specimens were tested for each solution time, and the final values were averaged. Metallographic samples were prepared from the gage parts of the tensile test bar. After etching in 0.5% HF solution, the microstructure was observed using an optical microscope (OLYMPUSBX-60M), then, etched deeply in 7% HF solution for an appropriate time to observe the variation of the morphology of Si using SEM.

1.3 Quantitative metallographic measurement

Quantitative metallographic analysis software was used to get the morphological parameters of Si particles (see Fig.1). At least 15 fields of view from a single specimen were recorded randomly by optical microscope and converted to digital image to be analyzed. Every datum obtained represents the average of 15 fields of view. The following morphological parameters were determined: ① Equivalent diameter is the diameter of a circle whose area is equal to the area of a measured particle; ② Shape factor (SF): $SF = 4\pi A/P^2$ [20], where 4π is a normalized constant, A is the area of a particle, P is the perimeter of a particle.

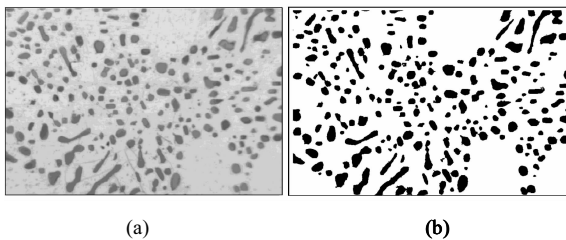


Fig.1 Quantitative metallographic analysis for eutectic Si. (a) Original image; (b) Binary image

2 Result and Discussion

2.1 Variation of eutectic Si morphology

As shown in Figs.2 (a) and (b), the Sr-modified

eutectic Si in the as-cast sample are fine fibers in which many “bottle-necks” appear in the trunk and branch of Si fibers while the root or end of Si fibers are rounded and smooth. As investigated earlier^[11, 12], with small additions of Na or Sr, the external surfaces of these Si fibers are rough or microfaceted, containing a very high twin density on up to four $\{111\}$ systems. The preferred growth axis of Si fibers is then $\langle 100 \rangle$ direction, with symmetrical branching in $\langle 211 \rangle$ directions. The consequence of this multiple twinning appears to allow anisotropic growth of Si in many directions simultaneously.

The variation of Si morphology during the initial solution period (250 min) is shown in Figs.2 (c) to (g). Si fibers undergo stubbing, necking, fragmentation and growth, and the four processes can be thought to occur simultaneously with no distinct order in time series in the present study. Up to 250 min, almost all the Si fibers obviously fragmented. It can be clearly observed from Fig.2 (d) that necking occurs at some specific positions, that is, at the branching and “bottle-neck” as well as at the unsubstantial part in the trunk of Si fibers. A similar result was observed by Zhu^[21]. It is thought that these positions relate to the twin crystals, due to a crystal defect where atoms are ranged in fault locations, which leads to an unstable energy state. Therefore, necking and dissolution separation will firstly occur at these positions due to the coupled effect of thermal flux, surface energy and curvature, i.e., the system tries to reduce excess surface area to the minimum possible. Si particles present the growth mode of regularizing and spheroidizing, and tend to become blunter and rounder. From the above observation, the variation of Si morphology with solution time, to a great extent, is determined by the as-cast Si morphology, i.e. by the modifier agent selected, modification processing and cooling conditions, etc.

During the middle solution period (250 to 400 min), the shape and size of Si particles undergo no significant changes, and the growth rates of Si particles become relatively slow while the degree of spheroidizing heightens, as shown in Figs.2 (g) and (h). This indicates that the dissolution and diffusion of eutectic Si tend towards equilibrium during these periods. As the solution proceeds, after 600 min, the morphology of Si particles is not as satisfactory as expected, and presents in the form of angle-shaped and faceted characteristics.

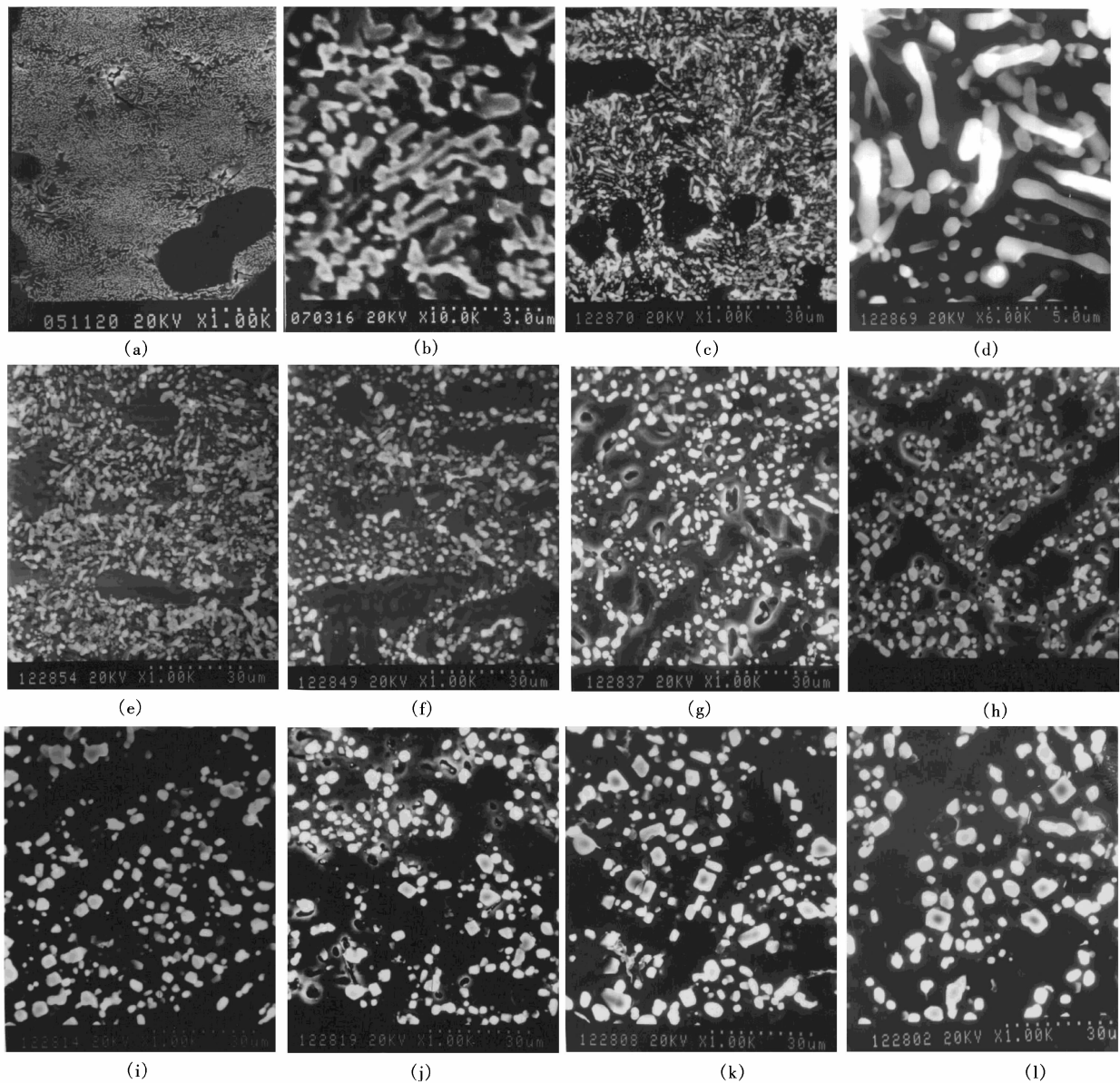


Fig.2 Variation of eutectic Si morphology with solution time at 535 °C. (a) As-cast; (b) High magnification of (a); (c) 40 min; (d) High magnification of (c); (e) 60 min; (f) 100 min; (g) 250 min; (h) 400 min; (i) 600 min; (j) 800 min; (k) 1 500 min; (l) 2 000 min

2.2 Faceted characteristics and lap

As mentioned above, a considerable quantity of Si particles with the angle-shape and block can be seen in Figs.2(i) to (l), especially in Figs.2(k) and (l). Figs.3 (a) and (b) are local higher magnification morphology of Si particles with faceted characteristics. According to the minimized surface energy principle, it is rational to believe that the eutectic Si particles grow spherical morphology. However, the present observation indicates that Si atoms have a preferred position and array in some specific orientations during the attachment to particle surface. Therefore, the Si particles display faceted characteristics.

Besides, it is also found that the Si particles with

faceted characteristics are interconnected with each other; within these connections a larger touching area and clear intersection lines can be observed, as shown

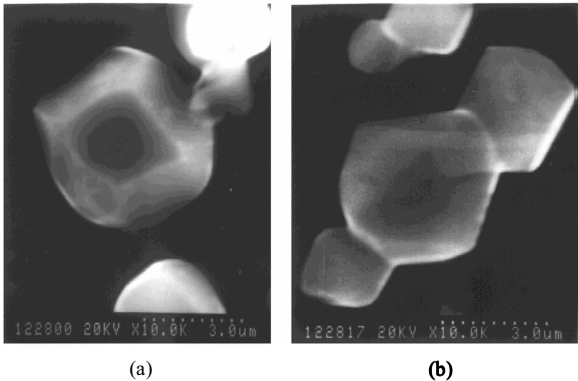


Fig.3 Facets and lap of Si particles in the final solution periods

in Fig.3(b). Such an intact lap suggests that the crystal growth meets some request, i.e. the arrays of atoms on the surfaces of these adjacent particles must be identical or similar in order to join together. If so, it further supports that the Si crystal grow along some preferred orientations. Another possible explanation is that the long Si rods do not completely dissolve into separate parts and still remain coarse. Based on the above observation and analysis, it is difficult to explain the formation of the faceted feature and lap. It requires future investigation by transmission electron microscope (TEM) to reveal the growth behavior of Si phase in the solution treatment.

2.3 Quantitative metallographic analysis

The variation of shape factors for Si particles with solution times is plotted in Fig.4. After 20 min, the SF is about 0.650, and varies from 0.756 for the solution time of 100 min, to about 0.900 for the solution time of 250 min. At about 500 min, the SF is up to 0.926, and the shape of Si particles approximates a circle and tends to stabilize. The values of the SF indicate that faster rates of spheroidization can be observed during the initial periods than during the middle or final periods, and is consistent with the evolution of Si morphology. After 600 min, as the solution time increases, the SF of Si particles does not increase as expected, but slightly decreases. This is related to the facets and lap of Si particles in the final solution periods. Hence, excessive solution time deteriorates the morphology of Si particles, instead of improving it.

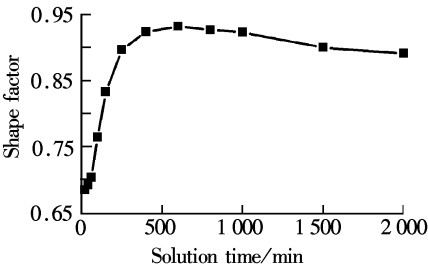


Fig.4 Variation of shape factor of Si particles with solution time at 535 °C

The variation of the cubic with average equivalent radii with the solution time is plotted in Fig.5. It can be divided into two stages. During the first stage from 250 to 400 min, the growth rate of Si particles is relatively slow because the dissolution and diffusion of Si particles tend to equilibrium. The second stage begins from 600 min, in which the growth of Si particles is controlled by diffusion and the growth of the larger Si particles depends on the consumptions of the smaller particles. The values of

R^3 are approximately linear with solution time as described by Lifshitz-Slyozov-Wagner equation (LSW) model^[22]: $R_t^3 - R_0^3 = At$, in which R_0 is the initial particle's equivalent radius at initial time, R_t is the particle's equivalent radius at some time, A is a constant, t is the solution time.

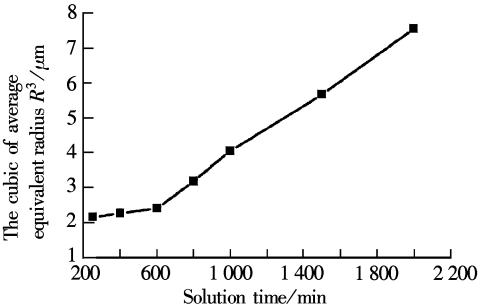


Fig.5 Coarsening process of Si particles with solution time

2.4 Correlation between mechanical properties with the morphology of Si particles

Fig. 6 clearly indicates that σ_b and δ are significantly linear with the SF and the straight lines are given by linear fit equations. The details are described in Tab.1. From these results it follows that the mechanical properties of modified Al-12.35% Si alloys under solution treatment (T_4) are linearly related with the SF of Si particles. It is suggested that the morphology of eutectic Si plays a very important role in improving the mechanical properties of the alloy.

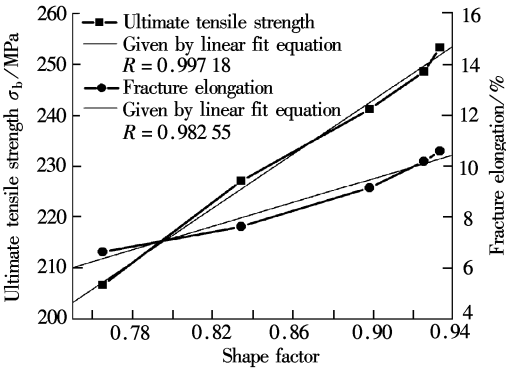


Fig.6 Correlation between the mechanical properties and the shape factor

Tab.1 Linear regression equations and correlation coefficients of mechanical properties with the SF of Si particles

	Regression equations	Correlation coefficients	Test of significance
Ultimate tensile strength	$Y = 6.28 + 263.27X$	0.997 18	$F = 354.89$
Fracture elongation	$Y = -12.01 + 24.19X$	0.982 55	$F = 75.09$

2.5 Fracture behavior

Fig. 7 shows the typical fractographs of

Al-12.35% Si alloy under different process conditions. As seen in Fig.7 (a), the major portion of the fracture surface consists of a complicated array of facets along certain crystallographic planes and some secondary cracks and tongue-shape patterns. The overall fracture is brittle in nature. The modified sample (Fig.7 (b)), on the other hand, shows a great amount of fine dimples and a smooth ripple pattern, which is the characteristic of a ductile feature. The dramatic change in the fracture mode can be attributed to the variations of the morphology and the size of the eutectic silicon particles.

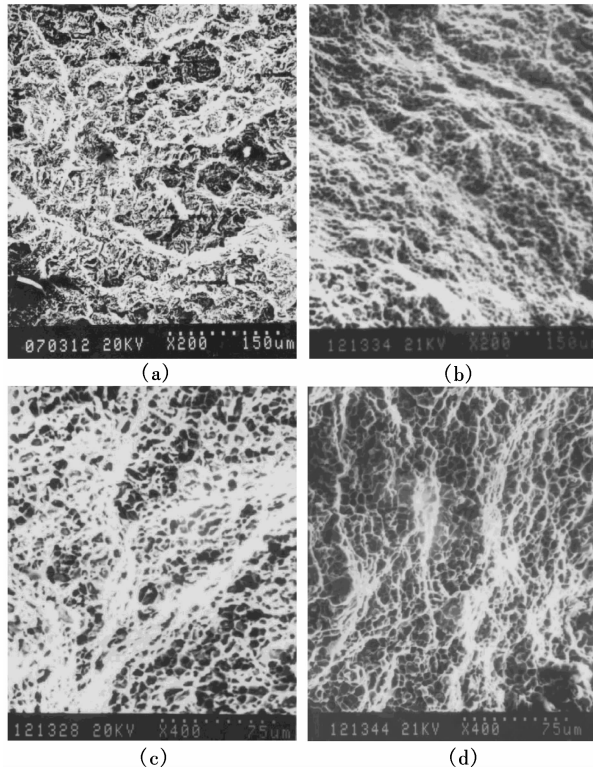


Fig. 7 Fractographs of Al-12.35% Si alloy under different process conditions. (a) Non-modified; (b) Sr-modified; (c) Sr-modified and solution time is 100 min; (d) Sr-modified and solution time is 400 min

The fractographs of the Sr-modified alloy after solution treatment for 100 min and 400 min at 535 °C are shown in Figs. 7 (c) and (d), respectively. A considerable quantity of finer dimples can be seen in both Fig.7(c) and Fig.7(d). Compared to Fig.7 (b), no significant change in the fracture mode can be detected after the modified alloy is solution treated. However, larger and deeper dimples are obviously observed in Fig.7 (b) and the ripples (surrounding the dimple) are finer and more complex, which indicates a better ductility. This is consistent with the results of the mechanical properties described above. It should be mentioned here that the change of Si particles tends to improve the stress field atmosphere between elastic rigid particles (Si particle) and ductile Al-

matrix, which improve the mechanical properties of the alloy.

In general, the failure of Al-Si alloy is accepted to occur in three stages^[7,9]: ① Silicon particles cracking at low strains (1% to 2%); ② As deformation proceeds, the individual voids grow and coalesce, and would link up to the main crack; ③ With the main crack's propagation, leading to final fracture. Refs.[5, 8] reported that particle morphology and orientation play a role in the strength of interaction between particles and plastic deformation. When the material is deformed, particles with a larger aspect ratio increase the strain hardening rate at low strains and tend to crack more readily, showing longer particles interacting more with plastic deformation than with rounder particles. Based on the present observations of fracture surface and the value of mechanical properties, the morphology of eutectic Si has a pronounced influence on fracture behavior.

3 Conclusions

1) In the initial solution periods (250 min), eutectic Si undergoes necking, stubbing, fragmentation and growth, and full separation of Si fibers is observed after a solution treatment of over 250 min. In the middle solution periods (250 to 400 min), the dissolution and diffusion of Si particles tend to equilibrium, the growth rates of Si particles are relatively slow. After 600 min the growth of Si particles is controlled by diffusion and follows the LSW model.

2) The faceted characteristics and lap of Si particles occur in the final solution periods; further investigation of the phenomenon is warranted.

3) Mechanical properties of the Al-12.35% Si alloy are linearly related to the SF of Si particles. It is suggested that the morphology of Si particles plays an important role in improving the mechanical properties of the eutectic Al-Si alloy.

4) In the present study, the fracture behavior is critically dependent on the morphology of eutectic Si.

References

- [1] Xiong Y C, Liu B C. Review and prospect of cast aluminum alloy [J]. *Special Casting & Nonferrous Alloys*, 1998(4): 1-4.
- [2] Ravi M, Pillai U T S, Pai B C, et al. A study of the influence of mischmetal additions to Al-7Si-0.3Mg alloy [J]. *Metall Mater Trans*, 1996, 27A(5): 1283-1292.
- [3] Liao H C. Investigation on microstructure refinement and mechanical properties of near-eutectic Al-Si alloys [D]. Nanjing: Department of Mechanical Engineering,

- Southeast University, 2000. (in Chinese)
- [4] Mondolfo L F. *Aluminum alloys: microstructure and properties* [M]. Translated by Wang Z T, et al. Beijing: Metallurgy Industry Press, 1988. 316 – 317. (in Chinese)
 - [5] Lebyodk M, Deschamps A, Brechet Y. Influence of second-phase morphology and topology on mechanical and fracture properties of Al-Si alloys [J]. *Mater Sci Eng*, 1997, **A234 – 236**: 481 – 484.
 - [6] Meyers C W, Saigal A, Berry J T. Fracture related properties of aluminum A357-T6 cast alloy and their interrelation with microstructure [J]. *AFS Trans*, 1983, **91**: 281 – 288.
 - [7] Wang Q G, Caceres C H. The fracture mode in Al-Si-Mg casting alloy [J]. *Mater Sci Eng*, 1998, **A241**: 72 – 82.
 - [8] Caceres C H, Davidson C J, Griffiths J R. The deformation and fracture behaviour of an Al-Si-Mg casting alloy [J]. *Mater Sci Eng*, 1995, **A27**: 171 – 179.
 - [9] Yeh Jien-Wei, Liu Wenpin. The cracking mechanism of silicon particles in an A357 aluminum alloy [J]. *Metall Trans*, 1996, **27**(11): 3558 – 3568.
 - [10] Mahmoud F, Hafiz, Toshiro Kobayashi. A study on the microstructure-fracture behavior relation in Al-Si casting alloys [J]. *Scripta Metallurgica*, 1994, **30**(4): 475 – 480.
 - [11] Lu Shu-zu, Hellawll A. The mechanism of silicon modification in aluminum silicon alloys: impurity induced twinning [J]. *Metall Trans*, 1987, **18A**(10): 1721 – 1733.
 - [12] Lu Shuzu, Hellawll A. Growth mechanisms of silicon in Al-Si alloy [J]. *J Crystal Growth*, 1985, **73**(2): 316 – 318.
 - [13] Pekguryuz M O, Gruzleski J E. Conditions for strontium master alloy additions to A356 melts [J]. *AFS Trans*, 1988, **96**: 55 – 64.
 - [14] Shamsuzzoha M, Hogan L M, Berry J T. Effects of modifying agents on crystallography and growth of silicon phase in Al-Si alloys [J]. *AFS Trans*, 1993, **102**: 999 – 1004.
 - [15] Meyers C W. Solution heat treatment effects in A357 alloys [J]. *AFS Trans*, 1985, **93**: 741 – 750.
 - [16] Shivkumar S, Ricci S, Apelian D. Influence of solution parameters and simplified supersaturation treatments on tensile properties of A356 alloys [J]. *AFS Trans*, 1990, **98**: 913 – 922.
 - [17] Shivkomar S, Ricci S, Steenhoff D, et al. An experimental study to optimize the treatment of A356 alloys [J]. *AFS Trans*, 1989, **97**: 791 – 810.
 - [18] Apelian D, Shivkumar S. Fundamental aspect of heat treatment of cast Al-Si-Mg alloy [J]. *AFS Trans*, 1990, **98**: 727 – 742.
 - [19] Pan E N, Hu J F, Fan C C. Solution-treatment conditions for optimal tensile properties in A357 alloy [J]. *AFS Trans*, 1996, **104**: 1119 – 1132.
 - [20] Castleman K R C, Kenneth R. *Digital image processing* [M]. Translated by Zhu Z G, et al. Beijing: Electron Industry Press, 1998. 247 – 428. (in Chinese)
 - [21] Zhu P Y, Liu O Y, Hou T X. Spheroidization of eutectic silicon in Al-Si alloys [J]. *AFS Trans*, 1985, **93**: 609 – 914.
 - [22] Verhecen J D. *Fundamentals of physical metallurgy* [M]. Translated by Lu G X, et al. Shanghai: Shanghai Science and Technology Press, 1980. 239 – 241. (in Chinese)

Al-Si 合金第二相形貌变化及其对断裂行为的影响

孙 瑜^{1,2} 陈 晋¹ 孙国雄¹

(¹ 东南大学材料科学与工程系, 南京 210096)

(² 盐城工学院材料科学与工程系, 盐城 224002)

摘要: 用光学显微镜和扫描电镜(SEM)观察 Al-Si 合金中硅相形貌在固溶过程中的变化, 并研究了此变化对合金力学性能和断裂行为的影响. 结果表明: 固溶初期 (250 min), 硅相发生缩颈、钝化、溶断并伴随长大; 在固溶中期 (250 ~ 400 min), 其形貌没有发生显著变化, 仅球化程度更高; 600 min 后, 硅相的长大是受扩散控制的粗化过程, 且符合 LSW 粗化模型; 同时由于出现棱角小面及搭接特征使硅相形貌有所恶化. 定量金相测量及回归分析说明硅相的形貌对合金的力学性能和断裂行为有显著影响.

关键词: Al-Si 合金; 硅相演变; 力学性能; 断裂行为

中图分类号: TG146.2⁺1; TG146.4⁺5